Applied Catalysis B: Environmental 101 (2011) 718–726

Contents lists available at ScienceDirect

Applied Catalysis B: Environmental

journal homepage: www.elsevier.com/locate/apcatb

Mesoporous-molecular-sieve-supported nickel sorbents for adsorptive desulfurization of commercial ultra-low-sulfur diesel fuel

Cigdem Sentorun-Shalaby, Shyamal Kumar Saha, Xiaoliang Ma*, Chunshan Song*

Clean Fuels and Catalysis Program, EMS Energy Institute, and Department of Energy & Mineral Engineering, The Pennsylvania State University, 209 Academic Projects Building, University Park, PA 16802, USA

ARTICLE INFO

Article history:
Received 12 June 2010
Received in revised form 7 October 2010
Accepted 9 November 2010
Available online 13 November 2010

Keywords:
Desulfurization
Adsorption
Diesel
Dibenzothiophene
Mesoporous silica
Nickel

ABSTRACT

A high-performance nickel-based sorbent was developed by loading nickel on a mesoporous molecular sieve, MCM-48, for adsorptive desulfurization (ADS) of commercial ultra low sulfur diesel (ULSD) for fuel cell applications. The prepared sorbents were characterized by the N_2 adsorption–desorption, X-ray diffraction (XRD), H_2 chemisorption, and transmission electron microscope (TEM), and the ADS performance was evaluated in a fixed-bed flow sorption system at 220 °C using a commercial ULSD with a sulfur content of 14.5 ppmw. Effects of the ultrasonic aid in incipient wetness impregnation (IWI), nickel loading amount and support materials on the sorbent performance were examined. It was found that the incipient wetness impregnation with the ultrasonic aid improved significantly the ADS performance of the sorbent by increasing the dispersion of nickel on the surface. Using MCM-48 as a support with 20 wt% nickel loading (Ni20/MCM-48) can lead to an excellent nickel-based sorbent with a breakthrough capacity of 2.1 mg-S/g-sorb for ADS of the ULSD at a breakthrough sulfur level of 1 ppmw. The alkyl dibenzothiophenes are likely adsorbed on the sorbent surface directly through an interaction between the sulfur atom and the exposed nickel atoms, and a part (~6%) of the adsorbed alkyl dibenzothiophenes react further with the surface nickel to release the corresponding hydrocarbons. The desulfurization reactivity of the alkyl dibenzothiophenes is dependent on not only the number, but also the size of the alkyl substituents at the 4- and 6-positions of alkyl dibenzothiophenes.

1. Introduction

Ultra-deep desulfurization of transportation fuels, such as diesel, gasoline, and jet fuel, has attracted a great deal of attention because of not only the stringent fuel specifications for the transportation fuels, but also the severe requirement of liquid hydrocarbon fuels with sulfur content less than 1 ppmw for fuel cell applications [1–6]. The current commercial ultra-low sulfur diesel (ULSD) with sulfur content less than 15 ppmw is a preferred fuel for the on-site and on-board fuel cell applications due to its high energy density, availability, safety and ease for production, delivery and storage by using the existing infrastructures. However, even in ULSD, in which the sulfur content is usually more than 10 ppmw, the sulfur content is still too high to be directly fed to the fuel processor to produce hydrogen for fuel cell applications [4,7,8] especially for the proton exchange membrane fuel cell (PEMFC) [5], as the sulfur compounds and H_2S produced from them in the fuel processor poison the reforming and water–gas-shift catalysts as well as the fuel cell stacks.

Currently, the sulfur removal from various liquid hydrocarbon streams is conducted by the catalytic hydrodesulfurization (HDS) process at 300–400 °C and 3–6 MPa hydrogen pressure with high hydrogen consumption in refineries. According to our previous study [2,9], if reducing the sulfur content in the current commercial ULSD from 15 ppmw to less than 1 ppmw by using the current hydrotreating technology, the catalyst bed volume or the catalyst activity must be about 68% higher than that currently used in refineries, as the remaining sulfur compounds in the commercial ULSD are the most refractory sulfur compounds. As is well known, the increase in both volume of the high-temperature and high-pressure reactor and the catalyst amount is very costly. Working at high temperature and high pressure also limits the usage of the HDS process in the on-site and on board desulfurization due to the complication and safety of the process. Therefore, it is desired to develop a novel technology for ultra-deep desulfurization of ULSD for fuel cell applications.

Many new approaches for ultra-deep desulfurization of liquid hydrocarbon fuels have been reported in the literature [1–3]. Among them the adsorptive adsorption on the nickel-based sorbents is promising and has attracted a great deal of attention due to the high capacity and selectivity without using hydrogen gas [10–19]. The nickel-based sorbent, such as Raney–Nickel, has

* Corresponding author. Tel.: +1 814 863 8744; fax: +1 814 863 7432.
E-mail addresses: mxx2@psu.edu (X. Ma), csong@psu.edu (C. Song).

0926-3373/$ – see front matter © 2010 Elsevier B.V. All rights reserved.
doi:10.1016/j.apcatb.2010.11.014

been used for desulfurization in organic synthesis for a long time [10,20,21]. Ma et al. reported that the nickel-based sorbent was very efficient in selective removal of some sulfur compounds, such as thiophene, benzothiophene and their alkyl substituted derivatives, from gasoline [11,13]. Velu et al. studied the desulfurization of the light JP-8 with 380 ppmw of sulfur at 220 °C on a $Ni/SiO_2–Al_2O_3$ sorbent with Ni loading of 55 wt% [12], and got a breakthrough capacity of 13.5 mg-S/g-sorbent at a breakthrough sulfur level of 30 ppmw. Kim et al. found that the lower sorption selectivity of the $Ni/SiO_2–AlO_2$ sorbent for 4,6-DMDBT than DBT, and pointed out that the alkyl groups at 4- and/or 6-positions have strong steric hindrance toward the sorption [14]. A study reported later by Hernández et al. [18] in desulfurization of a model fuel over a $Ni/SiO_2–Al_2O_3$ sorbent also supports the finding by Kim et al. [14]. In order to improve the sorption performance of the nickel-based sorbents, Ko et al. and later Park et al. reported using the SBA-15-supported nickel sorbent with different nickel loadings for desulfurization of a commercial diesel fuel with 240 ppmw of sulfur [15,16]. They found that the SBA-15-supported nickel sorbent with 30 wt% of Ni loading gave the best breakthrough capacity of 1.7 mg-S/g-sorbent at a breakthrough sulfur level of 10 ppmw. However, when using the same SBA-15-supported nickel sorbent for desulfurization of a commercial ULSD with 11.7 ppmw of sulfur, they found that the breakthrough capacity was only 0.47 mg-S/g-sorbent. Thus, the capacity of the nickel based sorbent needs to be improved for the practical application in the on-board and on-site desulfurization of ULSD for fuel cell systems.

The objective of the present study is to improve the ADS performance of the nickel-based sorbents for ULSD by increasing the dispersion of nickel in the nickel-based sorbent, and get better insight into the ADS mechanism of the refractory sulfur compounds on the sorbent. Different mesoporous molecular sieves (SBA-15 and MCM-48) and ultrasonic aid technique were used to increase the nickel dispersion. The ADS performance of the prepared sorbents was evaluated in a fixed-bed flow sorption system at 220 °C using a commercial ULSD with sulfur content of 14.5 ppmw. Effects of the ultrasonic aid in the incipient wetness impregnation (IWI), nickel loading amount and support materials on the ADS performance of the sorbents were examined. The prepared sorbents were characterized by the N_2 adsorption–desorption at −196 °C, X-ray diffraction (XRD), H_2 chemisorption, and transmission electron microscope (TEM), and the results were correlated with their ADS performance. The ADS selectivity and mechanism for the sulfur compounds on the nickel-based sorbent were also discussed on the basis of the detailed analysis of the sulfur compounds and the formed hydrocarbons in the treated fuels.

2. Experimental

2.1. Preparation of mesoporous-molecular-sieve-supported Ni sorbents

The SBA-15 was synthesized according to the procedure reported by Wang et al. [22,23] based on the method initially reported by Zhao et al. in 1998 [24]. Typically, a homogeneous mixture, which was composed of triblock copolymer Pluronic of P123 (EO20PO70EO20, MW = 5800, Aldrich) and tetraethyl orthosilicate (TEOS) in hydrochloric acid, was stirred at 40 °C for 20 h, and then further treated at 100 °C for 24 h. The solid product was filtered and washed with plenty of water, dried in an oven at 100 °C, and subsequently calcined at 550 °C for 6 h under an air flow (100 ml/min).

MCM-48 was prepared from a mixture with the following gel composition: 1.0 SiO_2:0.5 NaOH:0.65 CTAB:62 H_2O:0.1 NH_4F using a similar procedure as described in the literature [25]. The resulting mixture was transferred into Teflon-lined stainless steel autoclave and crystallized at 120 °C for 1 day. The solid product was recovered by filtration, washed and dried at 120 °C overnight, and subsequently calcined at 550 °C for 6 h under an air flow (60 ml/min). The mesoporous-molecular-sieve-supported nickel sorbents were prepared using an incipient wetness impregnation (IWI) method. Tetrahydrofuran (THF) was used as a solvent to prepare the $Ni(NO_3)_2$ solution, as reported by Ko et al. [15,26]. The desired amount of $Ni(NO_3)_2{\cdot}6H_2O$ was dissolved in THF, and the solution was slowly added into the support material at room temperature under the mechanical stir or with ultrasonic aid in a VWR-Model 75T ultrasonic bath. For the ultrasonic aid case, after adding the solution, the mixture was kept in the ultrasonic bath for 3 h at room temperature. The mixture was then dried in an oven at 100 °C overnight. The dried samples were then reduced in situ in a fixed-bed reactor under a pure hydrogen gas flow at 550 °C for 4 h before use. The resultant samples were donated as Ni*x*/SBA-15, and Ni*x*/MCM-48, where *x* indicates the loading amount of nickel as metal in weight percentage (wt%).

All chemicals that were used in the preparation of the sorbents, including Pluronic (P123) (Mn: 5800), TEOS with a purity of 98%, THF with a purity of 99%, hydrochloric acid solution (HCl) with a purity of 37%, Cab-O-SilM5, tetramethyl ammonium silicate (TMAS), sodium silicate (SS) with a purity of 14% NaOH, 27% SiO_2, cetyltrimethylammonium bromide (CTAB), NH_4F with a purity of 99.99%, and nickel nitrate hexahydrate ($Ni(NO_3)_2{\cdot}6H_2O$), were purchased from Sigma–Aldrich (Allentown, PA), and were used as received without further purification.

2.2. Characterization of sorbents

The nitrogen adsorption–desorption at −196 °C was conducted using a Micromeritics ASAP2020 instrument. Samples were degassed for 3 h at 400 °C under vacuum ($P < 10^{-2}$ Pa) and subsequently analysed. The specific BET surface areas were determined from the N_2 adsorption at relative pressures of $0.05 < P/P_0 < 0.3$. The pore size distribution (PSD) was calculated from the adsorption branch of the N_2 physisorption isotherms employing the Barret–Joyner–Halenda (BJH) formula [27]. The total pore volumes (V_{Total}) were estimated from the volume of N_2 (as liquid) held at a relative pressure (P/P_0) of 0.98.

Some prepared sorbents were further characterized by X-ray diffraction (XRD) to get more structural information. XRD patterns were recorded by using a Pad V (Scintag, Inc., Cupertino, CA; currently Thermo Scientific) with CuKα1 radiation (λ = 1.54056 Å). X-ray diffraction patterns were collected in a continuous mode over two separate 2–θ ranges using different scan speeds. At low angle region, 0.5–6°, 2–θ scan was collected at a scan speed of 1 °/min, and at high angle region, 20–70°, 2–θ scan was collected at a scan speed of 2 °/min. The crystallite size of Ni on the sorbents was estimated by Scherrer equation.

Transmission electron microscopy (TEM) was obtained by using a JEOL EM-2010F with EDS from EDAX operating at accelerating voltage of 200 kV. The samples were prepared by dispersing the sorbent powder as slurry in acetone, which was then deposited and dried on a lacey carbon film on a Cu grid.

The H_2-chemisorption was performed using a Micromeritics AutoChem II 2910 instrument. About 40 mg of the sample was first pretreated in a quartz reactor under a pure H_2 flow at 550 °C for 2 h followed by purging with high-purity argon (Ar). After the sample was cooled to 50 °C, a H_2–Ar mixture with 5 vol% H_2 was introduced into the reactor. The consumption of H_2 was monitored by a thermal conductivity detector (TCD). The average particle size of the supported nickel was also estimated on the basis of H_2-chemisorption data according to the literature [28].

Table 1
Composition and properties of ultra-low sulfur diesel (ULSD).

Specific gravity	0.8374
Distillation (°C)	
IBP	166
T50	260
FBP	346
Cetane number (engine rating)	49.7
Flash point (°C)	63.9
Viscosity at 40 °C (cSt)	2.5
Pour point (°C)	−18
Cloud point (°C)	−12
Polycyclic aromatic hydrocarbon (GC–SFC, wt%)	6.9
Element analysis	
C (wt%)	86.8
H (wt%)	12.9
N (ppmw)	12
S (ppmw)	14.5

2.3. Evaluation of ADS performance of sorbents

Evaluation of the ADS performance of sorbents was conducted in a fixed-bed flow sorption system with a stainless steel column (4.6 mm I.D. × 150 mm length). About 0.8–1.1 g (depending on the packing density of the sorbent) of the dried sorbent (before reduction) was packed into a stainless steel column, and then was reduced in situ under a pure hydrogen flow at 550 °C for 4 h. When the temperature of the column was decreased to the room temperature under the hydrogen flow, the column was disconnected to the system and sealed quickly. After weighting the sealed column to estimate the weight of the reduced nickel-based sorbent by difference, the column was reconnected into the system for the subsequent ADS test. A commercial ULSD (or a model fuel) was fed into the column from the bottom by a HPLC pump. The adsorption temperature for evaluation of the sorbents was set at 220 °C, as the best temperature for ADS on the nickel-based sorbents was around 200–220 °C according to our previous studies [11–13]. The liquid hourly speed velocity (LHSV) of 4.8 h^{-1} was used in the test. The effluent fuel from the top of the column was periodically sampled at an interval of 15–20 min for analysis.

The ULSD with 14.5 ppmw total sulfur used in this study was from British Petroleum (BP). The composition and properties of the ULSD are listed in Table 1. A model fuel with 9.12 mmol/L of 4,6-DMDBT (corresponding to 400 ppmw of sulfur) and 9.12 mmol/L of *n*-tetradecane as an internal standard in *n*-decane was prepared and used in this study for test to determine the hydrocarbon products from desulfurization of 4,6-DMDBT on the nickel-based sorbent. *n*-Decane (anhydrous, ≥99%), 4,6-DMDBT with a purity of 97% and *n*-tetradecane (≥99%) were purchased from Sigma–Aldrich (Allentown, PA), and were used as received without further purification.

2.4. Analysis of the treated ULSD and model fuel

The total sulfur concentration of the treated fuel samples was analysed by using ANTEK 9000 series sulfur analyzer. The sulfur compounds in the treated and un-treated fuels were analysed by using a Hewlett-Packard gas chromatograph equipped with a sulfur-selective pulsed flame photometric detector (GC–PFPD). A Hewlett Packard 5890 series II gas chromatograph with a capillary column (XTI-5, Restek, bonded 5%, 30 m × 0.25 mm I.D. × 0.25 μm film thickness) and a split mode injector (ratio: 100:1) was used with ultra high-purity helium as a carrier gas. The oven temperature was initially set at 120 °C and ramped immediately at 6 °C/min to 170 °C, followed by a ramp at 20 °C/min from 170 to 290 °C, and held at 290 °C for 5 min. The injection sample volume was 1 μL. The temperature of both injector and detector in GC–PFPD analysis was kept at 290 °C. The identification of the sulfur compounds was conducted by comparison of the relative retention times with those reported in the literature [29,30].

The identification of the hydrocarbon products from the desulfurization of the model fuel on the nickel-based sorbent was carried out by combination of the gas chromatography–mass spectrometry analyses (GC–MS) and comparison of the retention times with those of some standard hydrocarbon samples, such as 3-methylbiphenyl (3-MBP), 3,3′-dimethylbiphenyl (3,3′-DMBP) and 3,4′-dimethylbiphenyl (3,4′-DMBP). The GC–MS analyzer consisted of a Shimadzu GC-17A gas chromatograph coupled with a Shimadzu QP-5000 mass spectrometer. The gas chromatograph was fitted with a fused silica capillary column (Rxi-5ms, 30 m × 0.25 mm I.D. × 0.25 μm film thickness) purchased from Restek. The ultra high purity helium was used as a carrier gas at a flow rate of 1 ml/min. The quantification of the hydrocarbon products was conducted by using a Hewlett-Packard gas chromatography equipped with a flame ionization detector (FID) and the same capillary column with *n*-tetradecane as an internal standard.

3. Results and discussion

3.1. Effect of ultrasonic aid on sorbent preparation

The sorbents with 20 wt% nickel on SBA-15 (Ni20/SBA-15) were prepared by the IWI method with and without the ultrasonic aid. Adsorptive performances of the two prepared Ni20/SBA-15 sorbents for desulfurization of the ULSD were evaluated at 220 °C and 4.8 h^{-1} LHSV in the fixed bed flow system. The breakthrough curves of the ULSD over two Ni20/SBA-15 sorbents are shown in Fig. 1. The breakthrough capacity of the Ni20/SBA-15 prepared by the IWI method without the ultrasonic aid was only 0.43 mg-S/g-sorb at a breakthrough sulfur level of 1 ppmw. This measured capacity is similar to that (0.47 mg-S/g-sorb) of the best Ni/SBA-15 sorbent reported by Park et al. for desulfurization of a ULSD with 11.7 ppmw sulfur [16]. The shapes of the two breakthrough curves are also similar. The breakthrough capacity of the Ni20/SBA-15 prepared by the IWI method with the ultrasonic aid was increased to 0.98 mg-S/g-sorb, which is about two times higher than that of the Ni20/SBA-15 without the ultrasonic aid and that of the Ni/SBA-15 prepared by Park et al. [16].

In order to understand why the ultrasonic aid preparation method improved the desulfurization performance of the Ni20/SBA-15, the two Ni20/SBA-15 sorbents prepared with and without the ultrasonic aid were characterized by XRD. The XRD patterns of the two samples are shown in Fig. 2 in comparison with that of SBA-15. XRD peaks for metallic nickel in the Ni20/SBA-

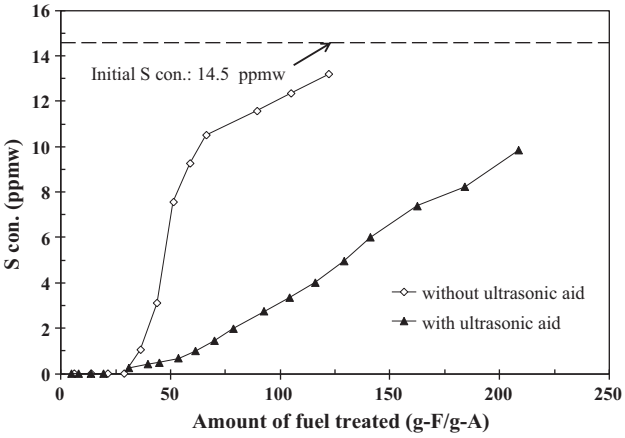

Fig. 1. Breakthrough curves of ULSD over Ni20/SBA-15 sorbents prepared with and without ultrasonic aid. Sorption condition: 220 °C and 4.8 h^{-1} of LHSV.

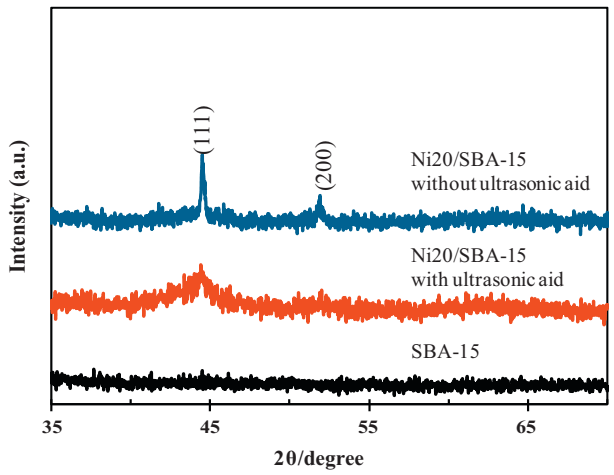

Fig. 2. XRD patterns of SBA-15 and the reduced Ni20/SBA-15 sorbents prepared by the IWI method with and without ultrasonic aid.

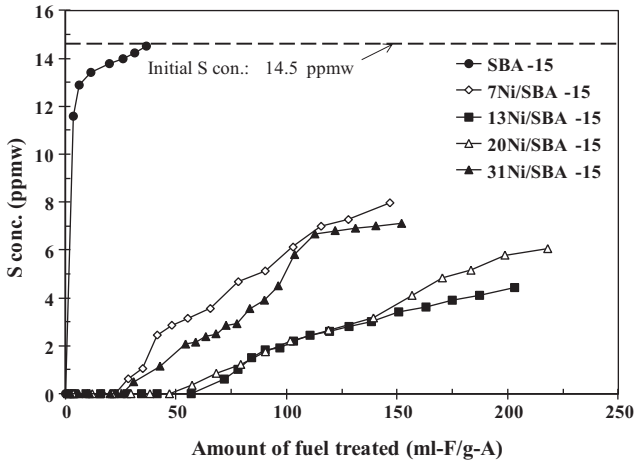

Fig. 4. Breakthrough curves of ULSD over Ni/SBA-15 sorbents with different Ni-loading. Sorption condition: 220 °C and 4.8 h^{-1} of LHSV.

15 prepared with the ultrasonic aid are much broader than those on with Ni20/SBA-15 without the ultrasonic aid, although the two samples had the same nickel loading. The particle size of nickel crystallites estimated according to the XRD patterns was 3.3 nm for the sample with the ultrasonic aid and 96 nm for the sample without the ultrasonic aid. The two Ni20/SBA-15 samples were further characterized by the H_2 chemisorption. The results show that the surface Ni in the Ni20/SBA-15 without the ultrasonic aid was only 0.0155 mmol/g, but in the Ni20/SBA-15 with the ultrasonic aid was 0.0305 mmol/g. Both the XRD and the H_2 chemisorption results indicate that the IWI method with the ultrasonic aid can significantly improve the dispersion of nickel on the mesoporous SBA-15 surface. As a result, the desulfurization performance of Ni20/SBA-15 was remarkably improved. Consequently, all mesoporous-molecular-sieve-supported nickel sorbents reported below were prepared by the IWI method with the ultrasonic aid.

In addition, XRD patterns of the synthesized SBA-15 and the Ni20/SBA-15 with the ultrasonic aid in the low angle region were also measured, as shown in Fig. 3. XRD patterns confirm that the synthesized sample is really SBA-15. In comparison of XRD patterns of the SBA-15 and the Ni20/SBA-15 with the ultrasonic aid, the intensity of SBA-15 signal of the Ni20/SBA-15 is weaker than that of the synthesized SBA-15 sample, implying that the loaded nickel was inside of the SBA-15 channels, which is consistent with the estimated particle size (3.3 nm) of the nickel crystallites in the Ni20/SBA-15.

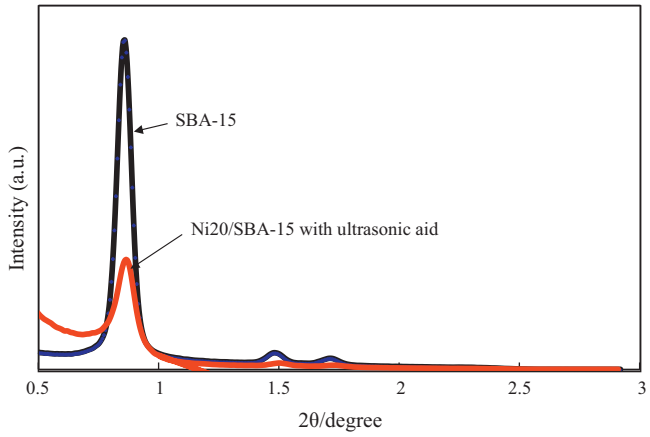

Fig. 3. XRD patterns of the synthesized SBA-15 and the reduced Ni20/SBA-15 prepared with ultrasonic aid in the low angle region.

3.2. Effect of nickel loading amount on desulfurization performance

In order to examine the effect of the loading amount of nickel on the desulfurization performance, four Ni/SBA-15 sorbents with different nickel loading amounts of 7, 13, 20, and 31 wt% were prepared by using the IWI method with the ultrasonic aid. The ADS performance of the four Ni/SBA-15 sorbents as well as SBA-15 for the ULSD was evaluated in the flow sorption system at 220 °C and 4.8 h^{-1} of LHSV. The breakthrough curves are shown in Fig. 4. SBA-15 shows almost no capacity for sulfur in comparison with Ni/SBA-15 sorbents, indicating that the nickel is a key component that interacts directly with the sulfur compounds. As it can be seen from Fig. 4, sorption capacities of Ni7/SBA-15 and Ni31/SBA-15 sorbents are much lower than those of Ni13/SBA-15 and Ni20/SBA-15 sorbents at a breakthrough sulfur level of 1 ppmw. The ADS capacity of the sorbents increases in the order of SBA-15 ≪ Ni7/SBA-15 < Ni31/SBA-15 < Ni13/SBA-15 ≈ Ni20/SBA-15. The breakthrough capacities of the four Ni/SBA-15 as well as SBA-15 were estimated and the values are listed in Table 2. The ADS capacity of Ni13/SBA-15 and Ni20/SBA-15 are 1.00 and 0.98 mg-S/g-sorb which are significantly higher than others.

The MCM-48-supported nickel sorbents with the nickel loading amount of 7, 13, 20, and 31 wt% were prepared by using the IWI method with the ultrasonic aid. Their sorption performances for desulfurization of the ULSD were evaluated in the flow sorption system at 220 °C and 4.8 h^{-1} of LHSV. The breakthrough curves for the four Ni/MCM-48 sorbents are shown in Fig. 5. The corre-

Table 2
The measured breakthrough capacities of sorbents at 220 °C and a breakthrough sulfur level of 1 ppmw.

Sorbent	Breakthrough capacities	
	mg-S/g-sorb	mg-S/ml-sorb
SBA-15	0.01	0.001
Ni7/SBA-15	0.47	0.056
Ni13/SBA-15	1.00	0.120
Ni20/SBA-15	0.98	0.118
Ni31/SBA-15	0.60	0.072
MCM-48	0.02	0.004
Ni7/MCM-48	0.32	0.106
Ni13/MCM-48	0.82	0.271
Ni20/MCM-48	2.10	0.693
Ni31/MCM-48	0.55	0.182
Raney Nickel	0.19	0.352
Ni55/SiO_2–Al_2O_3	0.41	0.314

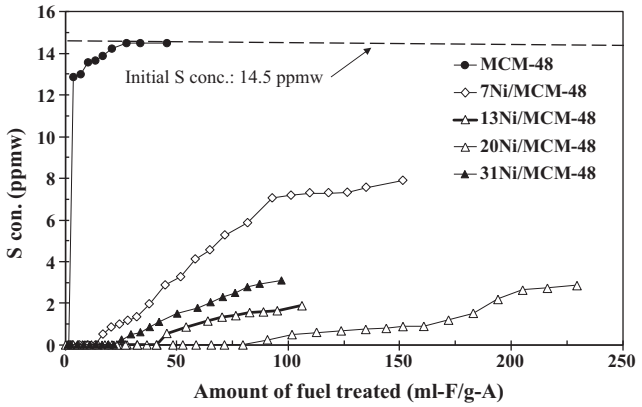

Fig. 5. Breakthrough curves of ULSD over Ni/MCM-48 sorbents with different Ni-loading. Sorption condition: 220 °C and 4.8 h^{-1} of LHSV.

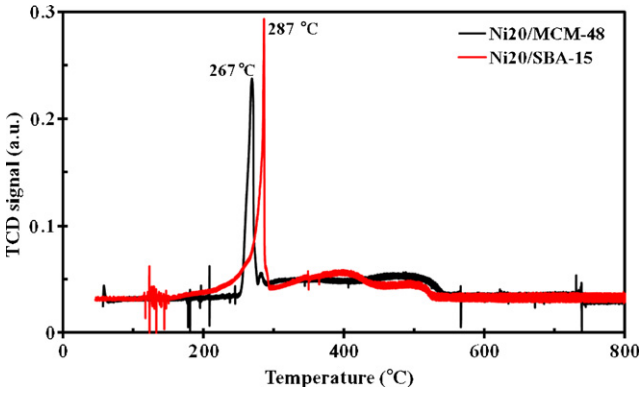

Fig. 6. TPR profiles of Ni20/MCM-48 and Ni20/SBA-15 samples before reduction.

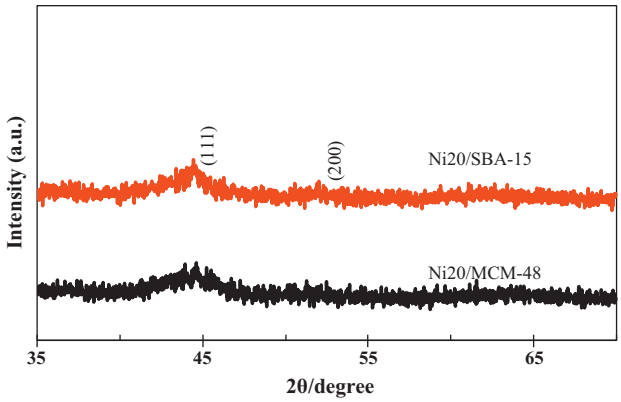

Fig. 7. XRD patterns of the reduced Ni20/SBA-15 and the reduced Ni20/MCM-48 sorbents prepared by IWI with ultrasonic aid.

sponding breakthrough capacities of the four Ni/MCM-48 sorbents at a breakthrough sulfur level of 1 ppmw are also listed in Table 2. The Ni7/MCM-48, Ni13/MCM-48 and Ni31/MCM-48 showed the breakthrough capacity similar to the Ni/SBA-15 with the same nickel loading. Interestingly, it was found that Ni20/MCM-48 gave the highest breakthrough capacity of 2.1 mg-S/g-sorb among the sorbents prepared in this study, which is higher than that of Ni13/SBA-15, the best Ni/SBA-15 sorbent obtained in this study, by a factor of 2. With increasing nickel loading, the measured breakthrough capacity increased firstly, and then decreased after passing a maxima value. This trend is consistent with the finding by Park et al. for Ni/SBA-15 and Ni/KIT-6. It seems that the continuous increase in the nickel loading may cause the agglomeration of the nickel particles and increase of the nickel crystallite size, thus results in the decrease of the active surface nickel atoms. It should be mentioned that the best loading amount of nickel in this study is 13–20 wt% for SBA-15 and 20 wt% for MCM-48, while the best loading amount of nickel in the study by Park et al. [16] is 30 wt% for both SBA-15 and KIT-6. The present study used the different diesel fuel and different sorbent preparation method may be the possible reasons. The further investigation is necessary to clarify it.

3.3. *Effect of the support materials*

In comparison of the desulfurization performance of Ni20/MCM-48 and Ni20/SBA-15 prepared in this study, the breakthrough capacity of the former is about 2 times higher that of the latter, although both sorbents have the same nickel loading. This indicates that the supports have a strong effect on ADS performance of the nickel-based sorbents. In order to clarify whether the reduction conditions of 550 °C for 4 h in a pure H_2 flow are good enough for reduction of all Ni in the sorbents, TPR of the dry Ni20/MCM-48 and Ni20/SBA-15 samples was conducted, and the obtained TPR profiles are shown in Fig. 6. These results indicate that both Ni20/MCM-48 and Ni20/SBA-15 can be reduced completely at 550 °C. The peak temperature of Ni20/MCM-48 sample for reducing the majority of nickel in it is lower than that of Ni20/SBA-15 by about 20 °C, implying that the former is easier to be reduced than the latter, probably due to the smaller particle size.

The XRD pattern of the Ni20/MCM-48 is shown in Fig. 7 in comparison with that of Ni20/SBA-15. The peak for nickel (1 1 1) in Ni20/MCM-48 is broader than that in Ni20/SBA-15. According to the XRD patterns, the estimated nickel crystal size for the former is 2.4 nm and for the latter is 3.3 nm (see Table 3). It is clear that the particle size of nickel crystallites in Ni20/MCM-48 is significantly less than that in Ni20/SBA-15. The further characterization of these two samples by the H_2 chemisorption shows that the nickel dispersion in Ni20/MCM-48 is about 35%, which is significantly higher than that of 21% in Ni20/SBA-15. The Ni particle size was also estimated on the basis of the H_2 chemisorption data. The estimated Ni particle size was 2.7 and 4.7 nm for Ni20/MCM-48 and Ni20/SBA-15, respectively, which is consistent with the results from the XRD patterns and the TPR profiles. The results from both XRD and the H_2 chemisorption show that MCM-48 gave better dispersion of nickel that SBA-15, although the estimated values from the H_2 chemisorption are slight higher than those from XRD, as listed in Table 3. Comparison of Ni20/MCM-48 and Ni20/SBA-15 indicates that structure of the support material plays an important role in determining the ADS performance of the nickel-based sorbents.

MCM-48 and Ni20/MCM-48 were also characterized by TEM. The TEM images are shown in Fig. 8. Fig. 8a confirms the three-dimensional branched network structure of the synthesized MCM-48. Fig. 8b shows the uniform distribution of the nickel particles with an average particle size about 2.5 nm in Ni20/MCM-48, which is consistent with the crystal size (2.4 nm) based on the XRD analysis. Since the average pore size of MCM-48 is around 2.7 nm (see Table 4), the majority of the nickel particles should be in the

Table 3
Metal particle size estimated on the basis of XRD, H_2 chemisorption and TEM analyses.

	XRD metal particle size (nm)	H_2 chemisorption metal particle size (nm)	TEM metal particle size (nm)
Ni20/SBA-15	3.3	4.7	
Ni20/MCM-48	2.4	2.7	2.5

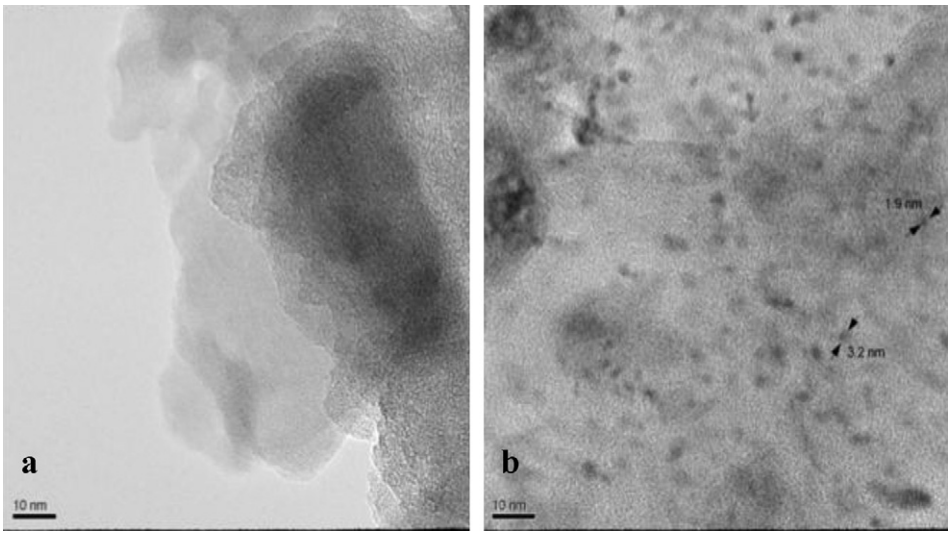

Fig. 8. TEM images of MCM-48 (a) and the reduced Ni20/MCM-48 (b).

MCM-48 channels, which results in the high dispersion of nickel on the MCM-48 surface. The three dimension pore structure, less pore size and higher surface area of MCM-48, as shown in Table 4, may be the reasons why the performance of Ni20/MCM-48 is much better than that of Ni20/SBA-15, in which SBA-15 has the one-dimension pore structure.

3.4. Comparison of ADS performance of different nickel-based sorbents

For comparison, the ADS performance of a commercial Raney Nickel (Raney 2800 from Aldrich and a Ni/SiO_2–Al_2O_3 with nickel loading of 55 wt% (Ni55/SiO_2–Al_2O_3) [12] was also evaluated at the same conditions. The breakthrough curves of the Raney Nickel and Ni55/SiO_2–Al_2O_3 in comparison with those of Ni20/SBA-15 and Ni20/MCM-48 sorbents are shown in Fig. 9. The measured breakthrough capacities of the Raney Nickel and Ni55/SiO_2–Al_2O_3 are also listed in Table 2. The breakthrough capacity on the basis of the sorbent weight increases in the order of Raney Nickel (0.19 mg-S/g-sorb) < Ni55/SiO_2–Al_2O_3 (0.41 mg-S/g-sorb) < Ni20/SBA-15 (0.98 mg-S/g) < Ni20/MCM-48 (2.1 mg-S/g). Ni20/MCM-48 gives the highest breakthrough capacity. If the results were compared on the basis of the sorbent volume, the order of breakthrough capacity is changed to Ni20/SBA-15 (0.12 mg-S/ml-sorb) < Ni55/SiO_2–Al_2O_3 (0.32 mg-S/ml-sorb) < Raney Nickel (0.35 mg-S/ml-sorb) < Ni20/MCM-48 (0.69 mg-S/ml-sorb), as the packing densities of the sorbents are quite different. On the basis of the sorbent volume the desulfurization performance of Ni20/MCM-48 is still the best sorbent among them. According to the present study, each kilogram of Ni20/MCM-48 is able to treat 170 L of the commercial ULSD with sulfur content of 14.5 ppmw to less than 1 ppmw at the outlet. The weight-based capacity of the Ni20/MCM-48 developed in this study is higher than that of the state-of-the-art nickel-based sorbent reported by Park et al. [16] by a factor of more than 4, which significantly improves the performance of the mesoporous-molecular-sieve-supported nickel sorbents for ADS of ULSD.

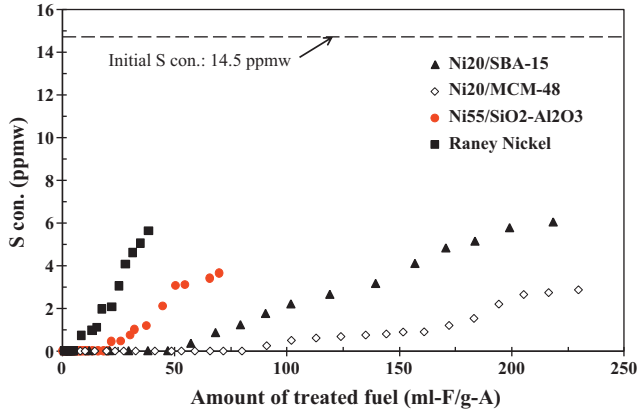

Fig. 9. Breakthrough curves of ULSD over Ni20/SBA-15, Ni20/MCM-48, Ni55/SiO_2–Al_2O_3, and Raney Nickel. Sorption condition: 220 °C and 4.8 h^{-1} of LHSV.

In order to clarify further why Ni20/MCM-48 exhibited the much better ADS performance than others, the H_2 chemisorption on the sorbents was conducted to measure the exposed nickel atoms in the sorbents. Assuming that each exposed Ni atom chemisorbs one hydrogen atom, thus the total number of the exposed Ni atoms was estimated by the H_2 chemisorption. The ADS breakthrough capacity of the sorbents as a function of the total number of the exposed nickel atoms in the sorbents is shown in Fig. 10. It clearly shows that the ADS breakthrough capacity increases with increasing the total number of the exposed Ni atoms. The results reveal that a large number of the exposed nickel atoms in Ni20/MCM-48

Table 4
Porous properties of the nickel-based sorbents and initial supporting materials on the basis of N_2 adsorption–desorption at −196 °C.

Sample	Surface area (m^2/g)	Total pore vol. (cm^3/g)	Micro-pore vol. (cm^3/g)	Meso-pore vol. (cm^3/g)	Pore size (nm)
MCM-48	1308	0.91	0.39	0.52	2.7
Ni20/MCM-48	503	0.32	0.16	0.16	2.6
SBA-15	889	1.24	0.36	0.88	6.4
Ni20/SBA-15	260	0.36	0.10	0.26	5.5
Raney Nickel	33	0.12	0.01	0.11	14.4
Ni55/SiO_2–Al_2O_3	157	–	–	–	–

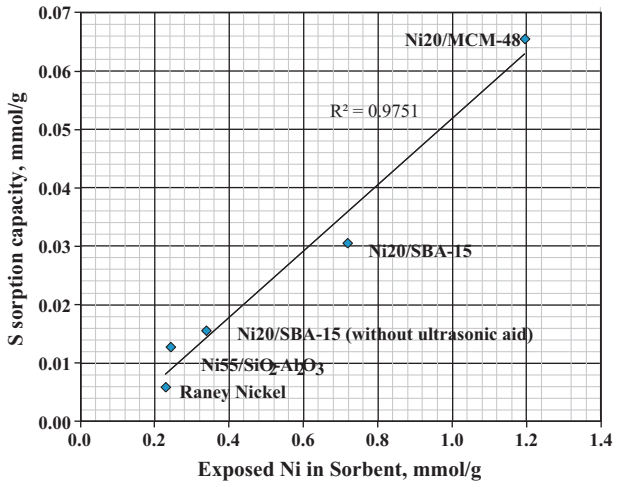

Fig. 10. ADS breakthrough capacity of the sorbents as a function of the total number of the exposed nickel atoms in the sorbents.

due to the high dispersion of nickel on MCM-48 results in the high breakthrough capacity of Ni20/MCM-48. The correlation data also suggest that each sulfur-containing molecule is adsorbed approximately on the twenty exposed nickel atoms. This value is much lower than the stoichiometry (from 0.48 to 1.09 for different crystal faces of nickel) of the S atoms per exposed Ni atom when the nickel surface is saturated by sulfur [31], indicating that the majority of the exposed Ni atoms still remain intact after the breakthrough, which will be further discussed in the following section.

3.5. Sorption selectivity and mechanism

Relatively little information is available regarding the sorption selectivity and mechanism on the nickel-based sorbents [17,19,32], although the nickel-based sorbents have been reported for ADS of liquid hydrocarbon fuels. In order to clarify the desulfurization selectivity of Ni20/MCM-48 for various sulfur compounds in the ULSD, the initial ULSD and the treated ULSD over Ni20/MCM-48 were analysed by GC–PFPD, and the sulfur compounds in them were identified by comparison of the relative retention times with those reported in the literature [29,30]. The GC–PFPD chromatograms of the initial ULSD and the treated ULSD with the assigned peaks are shown in Fig. 11. The major sulfur compounds in the ULSD with 14.5 ppmw sulfur are the alkyl DBTs with two alkyl substituents at the 4- and 6-positions respectively, such as 4,6-DMDBT, 4-ethyl,6-methyldibenzothiophene (4-E,6-MDBT), 2,4,6-trimethyldibenzothiophene (2,4,6-TMDBT), 4,6-diethyldibenzothiophene (4,6-DEDBT) and 6-ethyl,2,4-methyldibenzothiophene (6-E,2,4-DMDBT). This type of the sulfur compounds have been reported to be the most refractory sulfur compounds in gas oil [9], and thus, remained in the commercial ULSD.

It can be seen from the GC–PFPD chromatogram (Fig. 11) of the treated fuel corresponding to the collected sample at 107 ml-fuel/g-sorb, the first breakthrough sulfur compound was 4,6-DEDBT. By comparison of the GC–PFPD peak area of the sulfur compounds in the treated and initial fuels, it appears that the desulfurization selectivity of Ni20/MCM-48 decreases in the order of 4-MDBT > 4,6-DMDBT ≈ 2,4,6-TMDBT > 4-E,6-MDBT ≈ 6-E,2,4-DMDBT, > 4,6-DEDBT. It indicates that the desulfurization selectivity is dependent not only on the number of the alkyl substitutes at the 4- and 6-positions, but also on the size of the alkyl

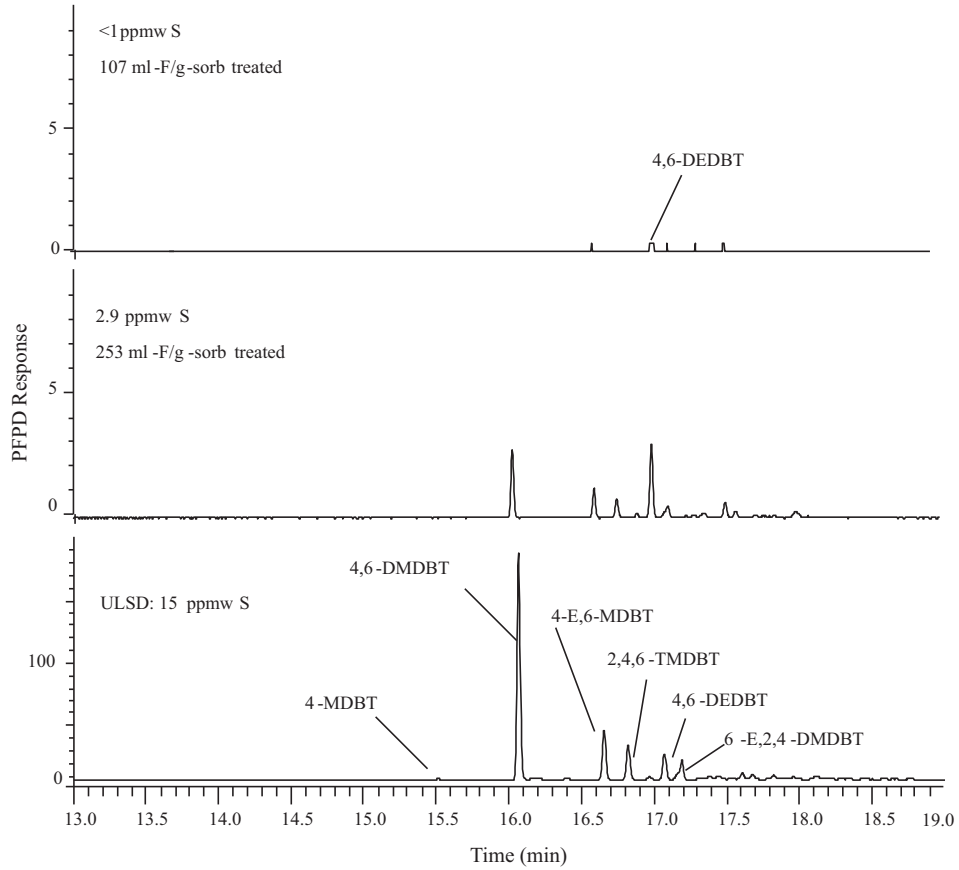

Fig. 11. GC–PFPD chromatographs of initial ULSD and the desulfurized ULSD samples over Ni20/MCM-48 at 220 °C, 4.8 h^{-1} of LHSV.

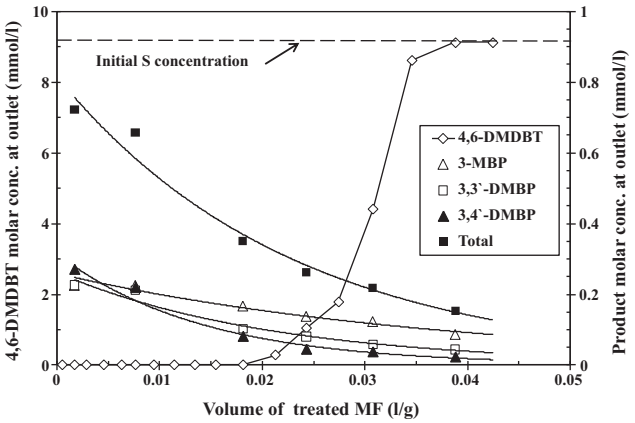

Fig. 12. The molar concentrations of the formed products and reactant 4,6-DMDBT as a function of the effluent volume.

substituents at the 4- and 6-positions. The lowest selectivity for 4,6-DEDBT among the all sulfur compounds in the ULSD can be ascribed to the two largest alkyl substituents (ethyl groups) at the 4- and 6-positions, respectively. This finding strongly suggests that the sorption of the sulfur compounds on the nickel-based sorbents is directly through an interaction between the sulfur atom in alkyl DBTs and the exposed nickel atom, and both the number and the size of alkyl substituents at the 4- and 6-positons have a strongly steric hindrance toward such interaction. This steric hindrance increases the interaction distance between the S atom and the nickel sites, resulting in a weaker interaction. Consequently, only the more exposed nickel atoms, such at those at the edges and corners, may be able to interact with the sulfur, resulting in a lower selectivity of the nickel-based sorbents for the DBTs with strong alkyl steric hindrance.

In order to understand further how the alkyl DBTs with the two alkyl substituents at the 4- and 6-positons are removed from the ULSD, ADS of a model fuel with 9.12 mmol/l of 4,6-DMDBT in *n*-decane over Ni20/MCM-48 was performed at 220 °C and 4.8 h^{-1} LHSV in the fixed-bed flow system. The formed products were identified by a combination of GC–MS analyses and comparison with standard samples, and quantified by GC–FID analysis. The major products detected in the effluent were 3-MBP, 3,3′-DMBP and 3,4′-DMBP. The molar concentrations of the formed products and the reactant 4,6-DMDBT as a function of the effluent volume are shown in Fig. 12. No sulfur compounds were detected when the effluent volume was less than 0.0195 l/g-sorb. The breakthrough capacity for 4,6-DMDBT was about 0.18 mmol-S/g-sorb (or 5.8 mg-S/g-sorb), and the saturation capacity was about 0.28 mmol-S/g-sorb (or 9.0 mg-S/g-sorb). The total molar concentration of the alkyl biphenyls was less than 0.8 mmol/l, which is much lower than the molar concentration of 4,6-DMDBT in the initial fuel (9.12 mmol/l). In comparison of the total molar number of the alkyl biphenyls in the effluent and the total sorbed sulfur molar number, it was found that the total molar number of the alkyl biphenyls in the effluent was only 5.9% of the total sorbed sulfur molar number, indicating that about 94% of the removed 4,6-DMDBT molecules or the formed hydrocarbon intermediates from them still stayed on the nickel surface. This value is much higher than that (33%) for the ADS of benzothiophene on a nickel-based sorbent even at 25 °C, reported previously by Ma et al. [11]. This is also different from the results observed by Hu et al., who found that thiophene molecules interacted strongly with the metallic nickel on Raney Nickel surface at −100 °C, and formed the surface nickel sulfides and released all the hydrocarbon part at 220 °C [32]. A possible reason may be that no steric hindrance of the alkyl substituents in thiophene and benzothiophene allows a strong interaction between the sulfur and the exposed nickel, which facilitates the S–C bond scission and releases the corresponding hydrocarbon. The results imply that the two methyl substituents at the 4- and 6-positions weaken remarkably the interaction between the sulfur atom and the exposed nickel atoms, resulting in the significant diminution of the S–C bond scission. Consequently, the 4,6-DMDBT molecules and/or the hydrocarbon intermediates adsorbed on the exposed nickel surface cover the nickel surface and block the way for contact of the subsequent 4,6-DMDBT molecules with the nickel surface, resulting in the low molar ratio of the sulfur to the exposed nickel, as mentioned in the previous section.

The presence of 3-MBP and 3,3′-DMBP and 3,4′-DMBP in the products implies that the sulfur atom in 4,6-DMDBT may be eliminated by three pathways, as shown in Fig. 13: direct S elimination (DE) from 4,6-DMDBT, isomerization of 4,6-DMDBT to form 3,6-DMDBT followed by the S elimination from 3,6-DMDBT (IFE) and demethylation of 4,6-DMDBT to form 4-MDBT followed by the S elimination from 4-MDBT (DFE). The similar concentration of 3-MBP and 3,3′-DMBP and 3,4′-DMBP detected in the effluent when the treated volume of the model fuel was less than 0.01 l/g indicates that the reaction rate for the three pathways was similar within this time. After passing 0.01 l/g of the treated volume, the concentration of 3-MDBT was significantly higher than others, suggesting that the surface reaction through DFE became dominant.

By combination of the results from the ADS selectivity of Ni20/MCM-48 for the different sulfur compounds in the ULSD and ADS of 4,6-DMDBT on Ni20/MCM-48, it is clear that the sulfur compounds are first adsorbed on the sorbent surface directly through an interaction of the sulfur atom in the compounds with the exposed nickel, and then, only a small part of the adsorbed sulfur compounds (∼6%) react further with the surface nickel through DE, IFE and DFE pathways to eliminate the sulfur atom by hydrogenolysis to form the surface nickel sulfide and release the corresponding hydrocarbon part from the surface due to the steric hindrance of the alkyl groups at the 4- and 6-positions. It should be mentioned that the ADS was conducted in the absence of hydrogen gas, the required

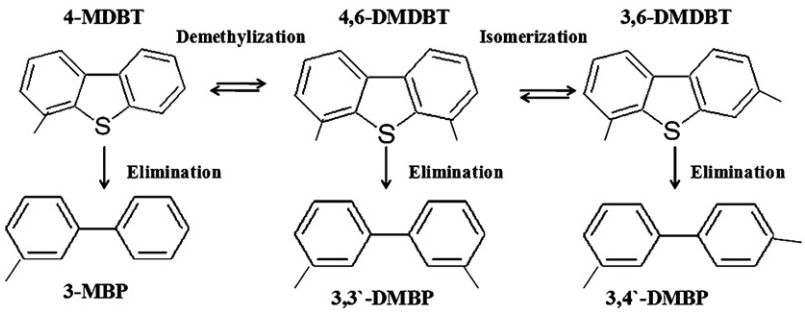

Fig. 13. Desulfurization pathways of 4,6-DMDBT on Ni20/MCM-48.

hydrogen for formation of the hydrocarbons may come from the nickel surface or other hydrocarbons in the fuel. The results suggest that introducing hydrogen to the nickel surface should accelerate the hydrogenolysis of the adsorbed sulfur compounds and release of the corresponding hydrocarbon part, and thus, provide more accessible nickel atoms to interact with other sulfur compounds, as also reported by Landau et al. [19].

In comparison of the ADS of the ULSD and the model fuel on Ni20/MCM-48, the ADS breakthrough capacity of Ni20/MCM-48 for the model fuel is about 5.8 mg-S/g-sorb, which is about 3 times higher than that for the ULSD. In addition of the higher sulfur concentration in the model fuel, there may be other two reasons: (1) the ULSD contains the more refractory sulfur compounds than 4,6-DMDBT in the model fuel, such as 4-E,6-MDBT 6-E,2,4-DMDBT, and 4,6-DEDBT which have larger size of the alkyl groups at the 4- and/or 6-positions. (2) The ULSD contains 12 ppmw of nitrogen compounds, which has the same magnitude as the sulfur compounds, and the nickel-based sorbents usually have the higher selectivity for the nitrogen compounds than for the sulfur compounds, as reported in our previous study [14].

4. Conclusions

A novel nickel-based sorbent for the reactive adsorption desulfurization of commercial ULSD was developed by impregnation of nickel precursor on a mesoporous silica, MCM-48. The sorbent preparation by the incipient wetness impregnation with the ultrasonic aid improved the ADS performance significantly, as the ultrasonic aid increased the dispersion of nickel on the support surface greatly. Using MCM-48 as a support with 20% nickel loading (Ni20/MCM-48) can lead to an excellent sorbent with a breakthrough capacity of 2.1 mg-S/g-sorb at a breakthrough sulfur level of 1 ppmw for sulfur removal from the commercial ULSD with 14.5 ppmw of sulfur. The correlation of the structure and performance of the nickel-based sorbents shows that the exposed nickel atoms play an important role in determining their sorption capacity. Study on the ADS mechanism indicates that alkyl DBTs are adsorbed on the sorbent surface directly through an interaction between the sulfur atom in the sulfur compounds and the exposed nickel atoms on the surface, and a part of the adsorbed alkyl DBTs (~6%) react further with the metallic nickel through DE, IFE or DFE pathways to form the surface nickel sulfides and release the corresponding hydrocarbon part from the surface. The desulfurization reactivity of the alkyl DBTs on the nickel-based sorbents is dependent not only on the number, but also on the size of the alkyl substituents at the 4- and 6-positions of DBTs. Among all sulfur compounds in the ULSD, 4,6-DEDBT has the lowest reactivity, which can be ascribed to the largest steric hindrance of the two ethyl groups at the 4- and 6-positions.

Acknowledgements

The authors are pleased to acknowledge the support of this work in part by the U.S. Department of Energy, National Energy Technology Laboratory under Contract No. DE-FC26-08NT0004396. The authors are grateful to Dr. Xiaoxing Wang for his help in preparation of SBA-15 and Chao Xie for his help in H_2 chemisorption analysis.

References

[1] C.S. Song, Catal. Today 86 (1–4) (2003) 211–263.
[2] C.S. Song, X.L. Ma, Appl. Catal. B: Environ. 41 (1–2) (2003) 207–238.
[3] E. Ito, J.A.R. van Veen, Catal. Today 116 (2006) 446–460.
[4] C.S. Song, Catal. Today 77 (2002) 17–49.
[5] R. Farrauto, S. Hwang, L. Shore, W. Ruettinger, J. Lampert, T. Giroux, Y. Liu, O. Ilinich, Annu. Rev. Mater. Res. 33 (2003) 1–27.
[6] Fuel Cell Handbook, 5th ed., EG&G Services, Parsons Inc. and Science Applications International Corporation, October 2000.
[7] D.C. Dayton, M. Ratcfliff, R. Bain, Milestone Completion Report, NREL/MP-510-30298, June 2001.
[8] M. Haberbauer, in: P. Lens, P. Westermann, M. Haberbauer, A. Moreno (Eds.), Biofuels for Fuel Cells, IWA, London, 2005, pp. 403–412.
[9] X.L. Ma, K. Sakanishi, I. Mochida, Ind. Eng. Chem. 33 (1994) 218–222.
[10] M. Nagai, H. Urimot, K. Uetake, N. Sakikawa, R.D. Goonzales, Polynuclear Aromatic Compounds, American Chemical Society, 1988.
[11] X.L. Ma, M. Sprague, C.S. Song, Ind. Eng. Chem. Res. 44 (2005) 5768–5775.
[12] S. Velu, X.L. Ma, C.S. Song, M. Namazian, S. Sethuraman, G. Venkataraman, Energy and Fuels 19 (3) (2005) 1116–1125.
[13] X.L. Ma, S. Velu, J.H. Kim, C.S. Song, Appl. Catal. B: Environ. 56 (1–2) (2005) 137–147.
[14] J.H. Kim, X.L. Ma, A. Zhou, C.S. Song, Catal. Today 111 (1–2) (2006) 74–83.
[15] C.H. Ko, J.G. Park, J.C. Park, H. Song, S. Han, S. Cho, J. Kim, Appl. Surf. Sci. 253 (2007) 5864–5867.
[16] J.G. Park, C.H. Ko, K.B. Yi, J. Park, S. Han, S. Cho, J. Kim, Appl. Catal. B: Environ. 81 (2008) 244–250.
[17] O. van Rheinberg, K. Lucka, H. Köhne, T. Schade, J.T. Andersson, Fuel 87 (2008) 2988–2996.
[18] S. Hernández, L. Solarino, G. Orsellob, N. Russo, D. Fino, G. Saracco, V. Specchia, Int. J. Hydrogen Energy 33 (2008) 3209–3214.
[19] M.V. Landau, M. Herskowitz, R. Agnihotri, J.E. Kegerreis, Ind. Eng. Chem. Res. 47 (2008) 6904–6916.
[20] W.B. Whalley, E.L. Anderson, F. Dugan, J.W. Wilson, G.E. Ullyot, J. Am. Chem. Soc. 77 (3) (1955) 745–749.
[21] M.T. Perlstei, M.Z. Atassi, S.H. Cheng, Biochim. Biophys. Acta 236 (1) (1971) 174.
[22] X.X. Wang, X.L. Ma, L. Sun, C.S. Song, Green Chem. 9 (2007) 695–702.
[23] X.X. Wang, Q.H. Zhang, S.F. Yang, Y. Wang, J. Phys. Chem. B 109 (2005) 23500–23508.
[24] D. Zhao, J. Feng, Q. Huo, N. Melosh, G.H. Fredrickson, B.F. Chmelka, G.D. Stucky, Science 279 (1998) 548–552.
[25] Y. Shao, L. Wang, J. Zhang, M. Anpo, J. Phys. Chem. B 109 (2005) 20835–20841.
[26] C.H. Ko, J.G. Park, S.-S. Han, J.-H. Park, S.-H. Cho, J.-N. Kim, Stud. Surf. Sci. Catal. 165 (2007) 881–884.
[27] E.P. Barrett, L.J. Joyner, P.P. Halenda, J. Am. Chem. Soc. 73 (1951) 373–380.
[28] W.B. Innes, in: R.B. Anderson, P.T. Dawson (Eds.), Experimental Methods in Catalytic Research, Academic Press, New York, 1968, pp. 44–46.
[29] T. Schade, J.T. Andersson, Energy Fuels 20 (2006) 1614–1620.
[30] T. Schade, J.T. Andersson, J. Chromatogr. A 1117 (2006) 206–213.
[31] C.H. Bartholomew, P.K. Agrawal, in: D.D. Eley, H. Pines, P.B. Weiez (Eds.), Advances in Catalysis, Academic Press, New York, 1982.
[32] H. Hu, M. Qiao, F. Xie, K. Fan, H. Lei, D. Tan, X. Bao, H. Lin, B. Zong, X. Zhang, J. Phys. Chem. B 109 (2005) 5186–5192.